

This appendix gives an impression of the Teigitsch hydropower system and its reservoirs. The appendix includes general data about the reservoirs and power plant system, pictures of the three reservoirs taken during the site visit on 28 March 2011 and pictures obtained from third parties.

A.1 Pack reservoir

The Teigitsch power plant system consists of three reservoirs in series. The highest reservoir is the reservoir Pack. Figure A-1 shows a top view of the left part of the Pack reservoir [VERBUND]. The Figures A-1.a to A-1.d are taken during the site visit on 28 March 2011. At that moment, the reservoir Pack was being emptied for inspection of the dam and power system and therefore important features as bank slopes could be seen. Figure A-1a clearly shows the downstream flow and the original width of the course. Figure A-1.b shows the banks of the reservoir. The most important figures are the Figure A-1c and Figure A-1d, which show the channel through the deposits formed by the drawdown. This channel is of similar kind to the channel formed in the Langmann reservoir during flushing. The pictures also show that the sediment consists mostly out of mud. This muddy sediment from the Pack reservoir will finally reach the Langmann reservoir, when both the upstream reservoirs are flushed.

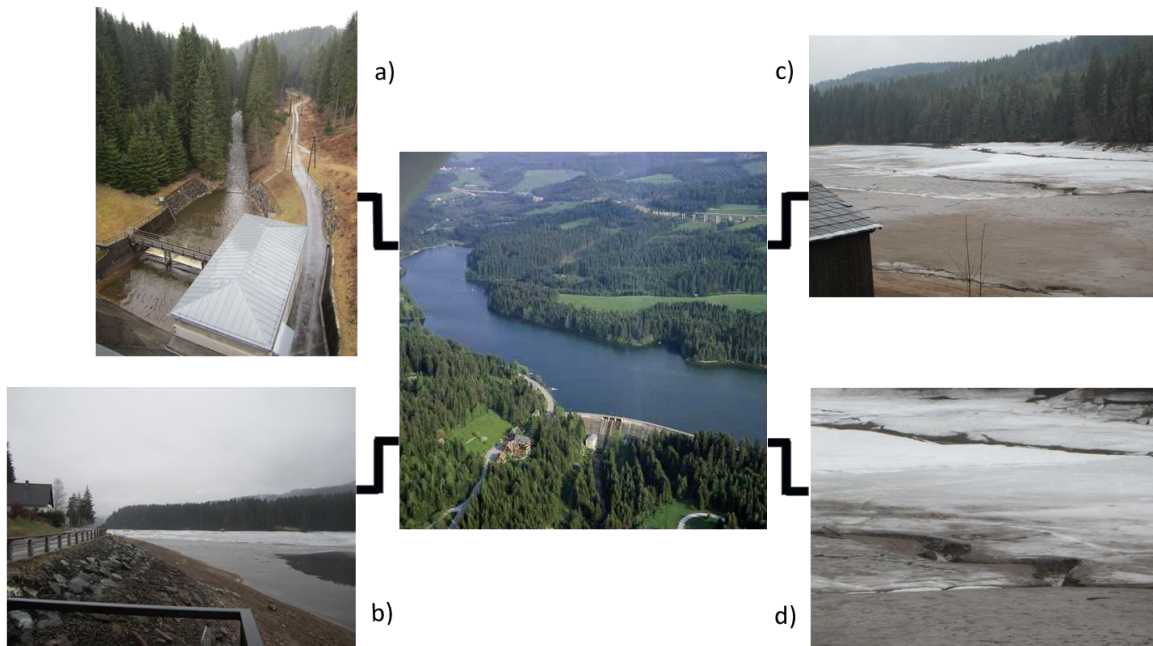


Figure A-1: Pack reservoir with a) downstream channel during drawdown b) side slope reservoir c) drawdown channel in upper left part reservoir and d) close-up of the drawdown channel.

A.2 Hierzmann reservoir

The reservoir Hierzmann is the second reservoir in the system. During the site visit, the Hierzmann water level was also partly drawn down in order to store the water coming from the upstream reservoir Pack and thereby preventing flooding of the reservoir. Figure A-2 shows a

top view of the reservoir Hierzmann [VERBUND]. Figures A-2b and Figure A-2c are taken during the site visit and show the Hierzmann dam and bank slopes of the reservoir Hierzmann. From the reservoir Hierzmann, there is no downstream flow, only some seepage water. The steep side slopes of the reservoir make it hard to control the flushing operations, especially the flushing concentrations. Figure A-2a⁷ is made on 2 April 2006, during the flushing operations. The figure shows the channel formation and the steep banks of the Hierzmann reservoir.

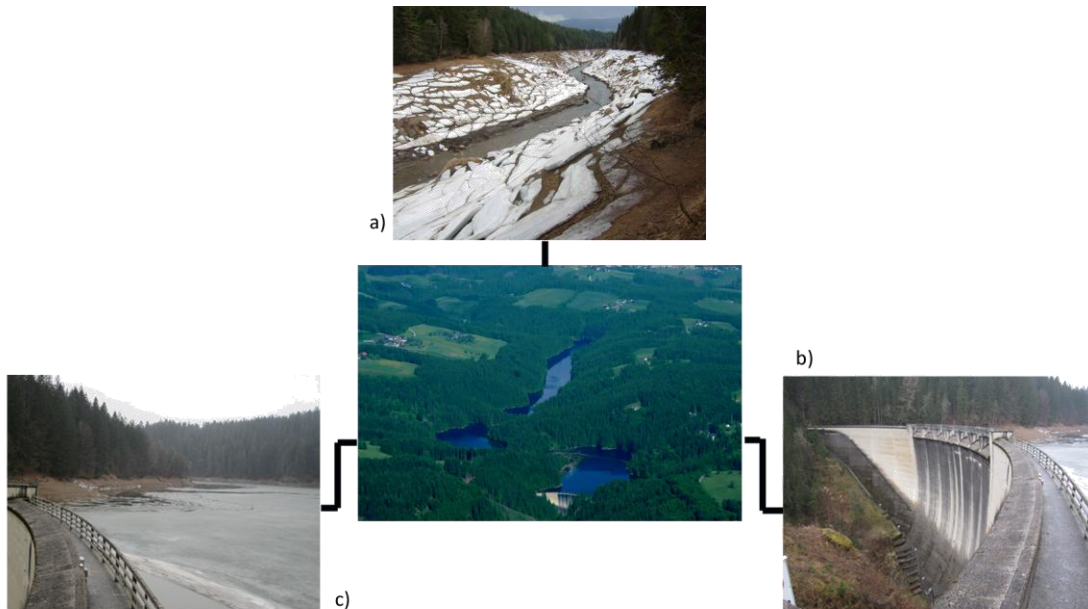


Figure A-2: Top view reservoir Hierzmann with a) channel after flushing b) the Hierzmann dam and c) steep side slopes of the Hierzmann reservoir.

A.3 Langmann reservoir

The reservoir Langmann is the lowest situated reservoir and the last in the series of three. In April 2009, a laser scan generated two images of the reservoir as well as a xyz.file. The laser scan was made after the initial drawdown of the reservoir. The two images show the reservoir with and without vegetation. Figure A-3 shows the image with vegetation and indication of reference points. The reservoir Langmann is closed by a concrete gravity dam of 85 metres long and 26 metres high. The inlet house is situated directly next to the dam. Approximately, halfway the reservoir an observation point is situated. Further upstream, the small river Niessenbach flows in the reservoir. The bridge upstream is indicated as the reservoir boundary. The bridge provides a good reference point and only a small part of the reservoir is excluded. The Langmann reservoir is therefore approximately 780 metres long and has an average width of approximately 50 metres. The water from the reservoir Langmann is let into a pipeline and transported to the Arnstein power plant downstream of the dam.

⁷ www.gps-tour.info/de/touren/detail.3058.html

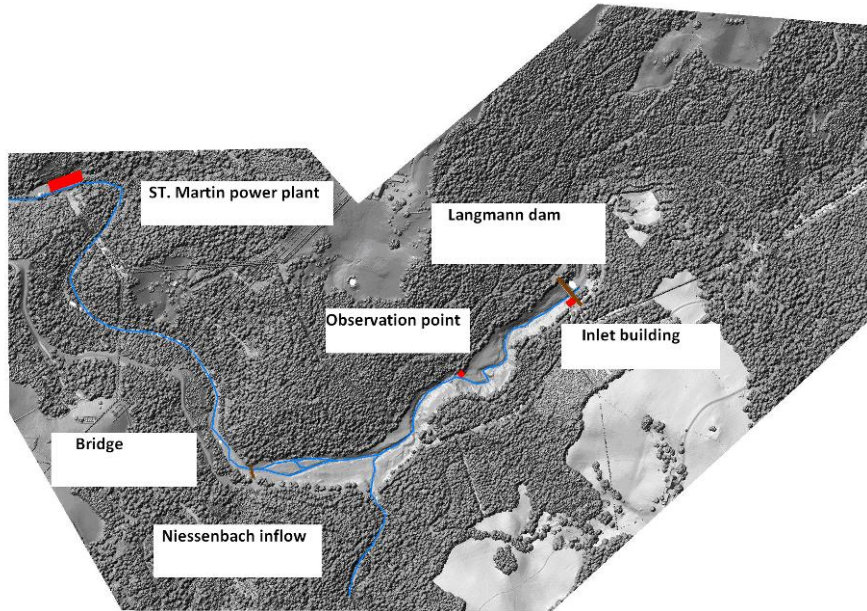


Figure A-3: Satellite image of Langmann reservoir with vegetation and reference points.

Figure A-4a shows the Arnstein powerhouse and Figure A-4b the pipeline system. Figure A-4c is a picture of a measurement device downstream of the powerhouse. This device measures the sediment concentration every five minutes. The device makes use of a laser beam.

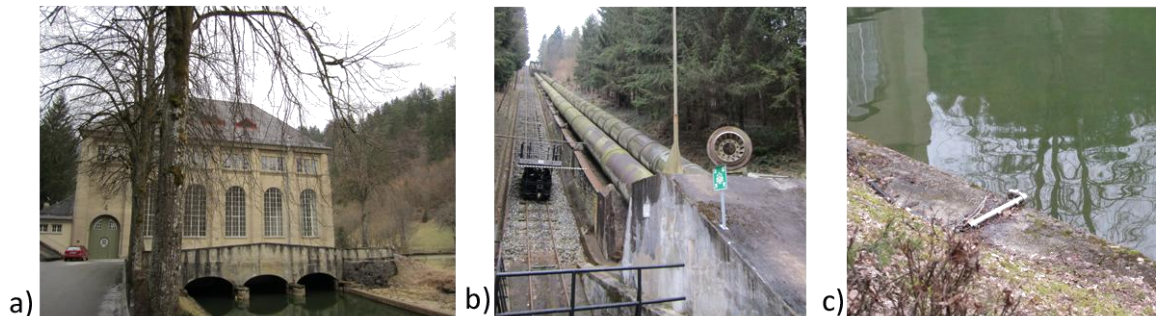


Figure A-4: Power plant Arnstein a) Power house b) pipeline from Langmann reservoir to power house c) measuring device for sediment concentration.

Figure A-5 gives an impression of Langmann reservoir. In Figure A-5d, the downstream river is shown. The river is almost completely dry and only contains some seepage water from the dam.

Figure A-6 gives the longitudinal on the power plant system. The reservoir Pack is the highest situated reservoir. Water from this reservoir is transported via the river Teigitsch to the Hierzmann reservoir. The water Hierzmann reservoir is transported via a pipeline to the underground power plant St. Martin. From the power plant the water is transported via a pipeline. The water flows in the river Teigitsch just before the Langmann reservoir. From the Langmann reservoir the water is also transported to the power plant by a pipeline. After the power plant Arnstein the water flows via an artificial channel to the power plant Teigitschmühle.

Table A.1 provides general data on the power plants and reservoirs of the Teigitsch power plant system.

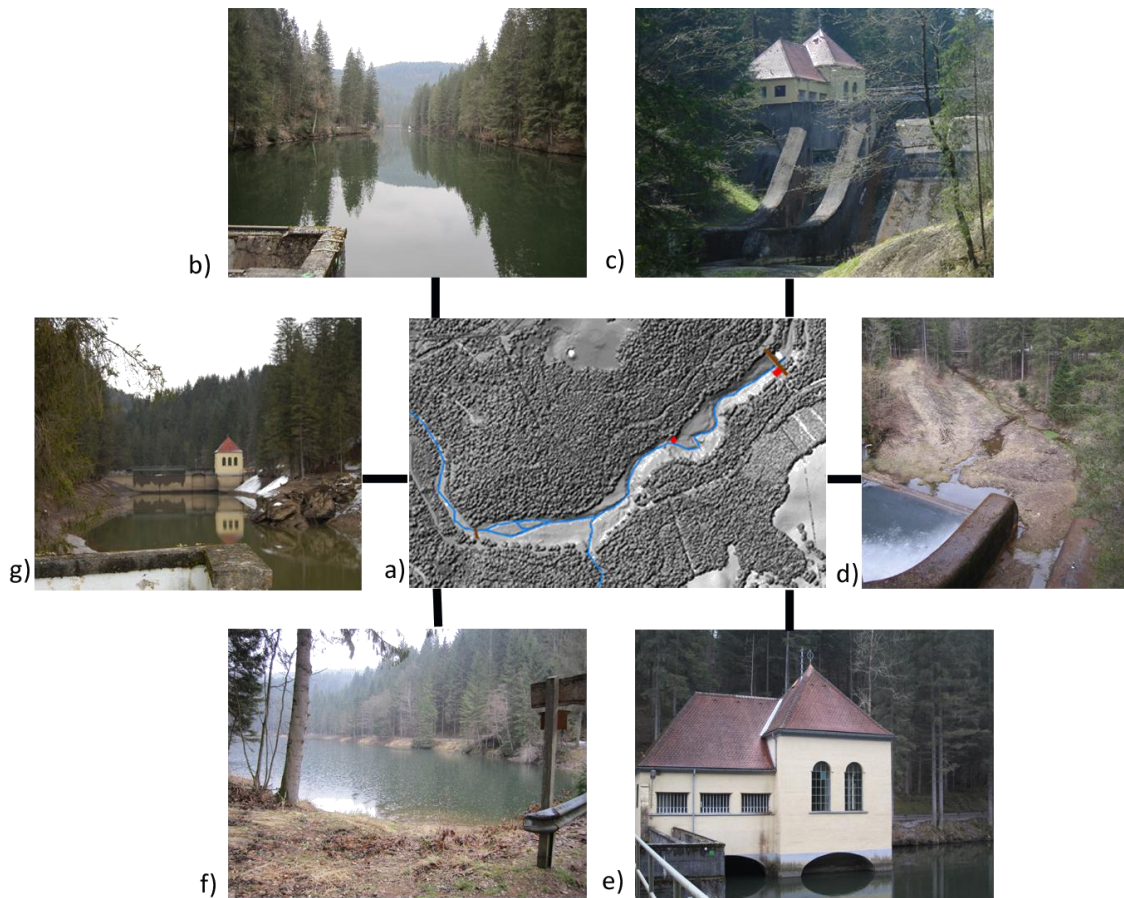


Figure A-5: Reservoir Langmann a) Top view of the reservoir b) impression reservoir looking upstream from the dam c) downstream side dam⁸ d) seepage from dam e) inlet house f) looking downstream from bridge g) looking downstream from observation point⁹.

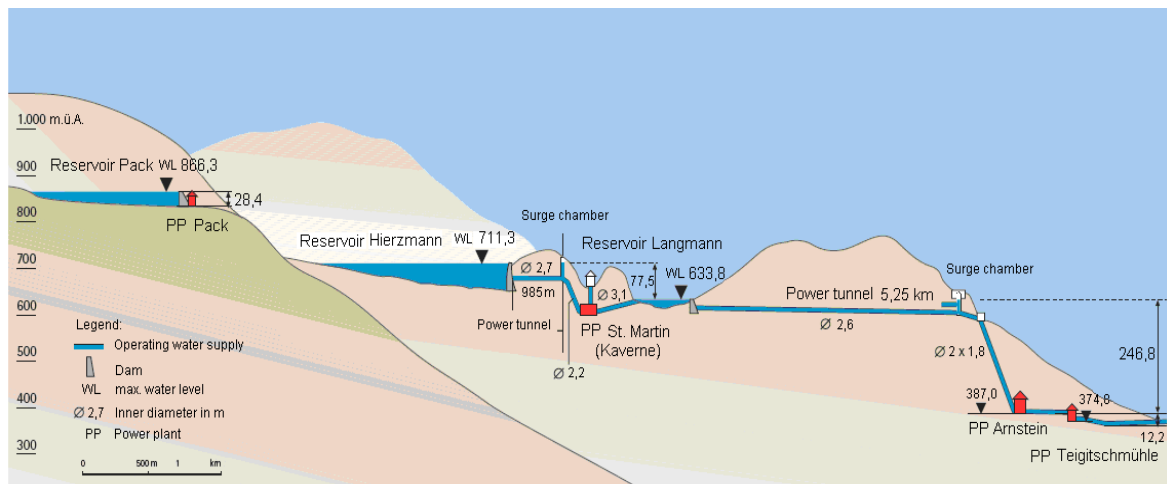


Figure A-6: Teigitsch hydropower plants, longitudinal view [TAMERL, 2006].

⁸ WWW.PANORAMIO.COM © QFWFQ-2

⁹ WWW.OPENCACHING.DE

Power plant	Pack	St. Martin	Arnstein	Teigitschmühle
Type of power plant	run-of-river power plant	annual storage power plant	annual storage power plant	run-of-river power plant
Commissioning	1931	1965	1925	1926
Catchment area	63 km ²	162 km ²	175km ²	170 km ²
Bottleneck capacity	800 kW	9,800 kW	30,000kW	1,200 kW
Standard capacity (average annual output from natural inflows)	1.8 GWh	15.5 GWh	50.0 GWh	2.0 GWh
Head	28.5 m	73.5 m	246.8 m	11.6 m

Reservoir and dam

Power plant	Pack	St. Martin	Arnstein	
Reservoir name	Pack	Hierzmann	Langmann	
Type of reservoir	annual storage reservoir	annual storage reservoir	Daily storage reservoir	
Retention water level m.ü.A.	866.3 m	711.3 m	633.8 m	
Minimum operating level m.ü.A.	843.6 m	678.3 m	624.3 m	
Net capacity	5.4 million m ³	7.1 million m ³	0.32 million m ³	
Type of dam	gravity dam	arch dam	gravity dam	
Height of dam	33.2 m	58.6 m	26.0 m	
Cress length	183 m	172 m	85 m	
Cress width	4.0 m	3,0 m	3.0 m	
Max.base width	24.0 m	17.,0 m	15.0 m	
Cubic meters of concrete	44,000 m ³	43,000 m ³	12,000 m ³	

Table A.1: General data on the power plant system of the river Teigitsch [TAMERL, 2006].

F.1 General

Delft3D solves the non-linear shallow water equations, which are derived from the 3-dimensional Navier Stokes equations for incompressible free surface flow. Delft3D models flow phenomena of which the horizontal length and time scale are larger than the vertical scales. The system of equations contains the horizontal equations of motion, the continuity equation and the transport equations for conservative constituents. In the vertical momentum equations the vertical accelerations are neglected, which leads to hydrostatic pressure equation. Vertical accelerations due to buoyancy effects and sudden variations in the topography are not taken into account in the model. The hydrostatic pressure equation becomes:

$$\frac{\partial P}{\partial \sigma} = -g \rho H \tag{F.1}$$

with:

- P = Hydrostatic water pressure [kg/(m.s²)]
- g = Acceleration due to gravity [m/s²]
- H = Total water depth [m]
- ρ = Water density [kg/m³]
- σ = Scaled vertical co-ordinate

The momentum equations in horizontal direction (ξ- and η-direction) are:

$$\begin{aligned} \frac{\partial u}{\partial t} + \frac{u}{\sqrt{G_{\xi\xi}}} \frac{\partial u}{\partial \xi} + \frac{v}{\sqrt{G_{\eta\eta}}} \frac{\partial u}{\partial \eta} + \frac{w}{d+\zeta} \frac{\partial u}{\partial \sigma} - \frac{v^2}{\sqrt{G_{\xi\xi}} \sqrt{G_{\eta\eta}}} \frac{\partial \sqrt{G_{\eta\eta}}}{\partial \xi} + \frac{uv}{\sqrt{G_{\xi\xi}} \sqrt{G_{\eta\eta}}} \frac{\partial \sqrt{G_{\xi\xi}}}{\partial \eta} - f_v = \\ - \frac{1}{\rho_0 \sqrt{G_{\xi\xi}}} P_\xi + F_\xi + \frac{1}{(d+\zeta)^2} \frac{\partial}{\partial \sigma} \left(v_v \frac{\partial u}{\partial \sigma} \right) + M_\xi \end{aligned} \tag{F.2}$$

and

$$\begin{aligned} \frac{\partial v}{\partial t} + \frac{u}{\sqrt{G_{\xi\xi}}} \frac{\partial v}{\partial \xi} + \frac{v}{\sqrt{G_{\eta\eta}}} \frac{\partial v}{\partial \eta} + \frac{w}{d+\zeta} \frac{\partial v}{\partial \sigma} - \frac{u^2}{\sqrt{G_{\xi\xi}} \sqrt{G_{\eta\eta}}} \frac{\partial \sqrt{G_{\xi\xi}}}{\partial \eta} + \frac{uv}{\sqrt{G_{\xi\xi}} \sqrt{G_{\eta\eta}}} \frac{\partial \sqrt{G_{\eta\eta}}}{\partial \xi} + f_u = \\ - \frac{1}{\rho_0 \sqrt{G_{\eta\eta}}} P_\eta + F_\eta + \frac{1}{(d+\zeta)^2} \frac{\partial}{\partial \sigma} \left(v_v \frac{\partial v}{\partial \sigma} \right) + M_\eta \end{aligned} \tag{F.3}$$

where:

- u,v,w = Fluid velocities in ξ ,η and z direction [m/s]
- d = Depth below some reference plane [m]

ζ	= Free surface elevation above reference plane	[m]
t	= Time	[s]
V_v	= Vertical eddy coefficient	[m ² /s]
P_η, P_ξ	= Hydraulic pressure gradients in ξ, η direction	[kg/m ² s ²]
F_η, F_ξ	= Turbulent momentum flux in ξ, η direction	[m/s ²]
M_η, M_ξ	= External source and sink of momentum in ξ, η direction	[m/s ²]
$\sqrt{G_{\eta\eta}}, \sqrt{G_{\xi\xi}}$	= Coefficient used to transform curvilinear to rectangular co-ordinates	[m]

The depth-averaged continuity equation is given by:

$$\frac{\partial \zeta}{\partial t} + \frac{1}{\sqrt{G_{\xi\xi}} \sqrt{G_{\eta\eta}}} \frac{\partial \left[(d + \zeta) U \sqrt{G_{\eta\eta}} \right]}{\partial \xi} + \frac{1}{\sqrt{G_{\xi\xi}} \sqrt{G_{\eta\eta}}} \frac{\partial \left[(d + \zeta) V \sqrt{G_{\xi\xi}} \right]}{\partial \eta} = Q \quad (\text{F.4})$$

$$Q = H \int_{-1}^0 (q_{in} - q_{out}) d\sigma + P - E \quad (\text{F.5})$$

where:

Q	= Global source of sink per unit of volume	[m/s]
q	= Local sources and sinks of water per unit of volume	[1/s]
P	= Precipitation	[m/s]
E	= Evaporation	[m/s]
U, V	= Depth averaged velocities in ξ, η directions	[m/s]

F.2 Grid

Delft3D is a numerical model based on finite differences, therefore the shallow water equations have to be discretized. The shallow water equations are discretized via the staggered grid approach. In a staggered grid not all parameters are defined at the same location in the numerical grid. The water level points are defined in the cell centre and the velocity components at the cell faces. It is important to understand the numbering of a staggered grid and the definition of a computational control volume. Figure F-1 shows the grid numbering and an example of a computational control volume.

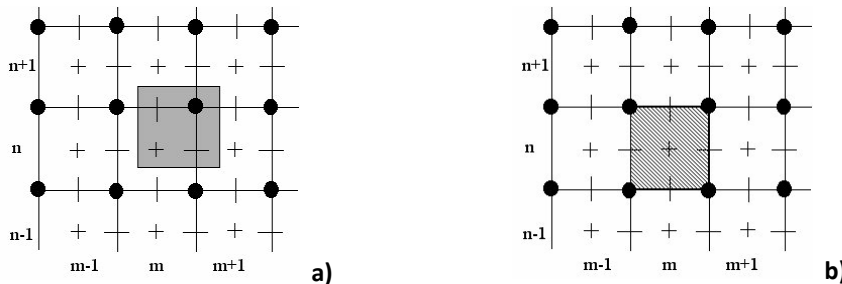


Figure F-1: Staggered grid with a) staggered grid cell and b) Computational control volume [DELTAES, 2010b].

In the figure the following is shown:

- +: water level, concentration of constituents, salinity, and temperature.
- : horizontal velocity component x, ξ, u, m direction.
- |: Horizontal velocity component y, η, v or n direction.
- Depth
- Full lines: the numerical grid
-  Staggered grid cell (items with the same array number (m,n))
-  Computational control volume

This grid must fulfil several criteria, namely:

- The grid must fit the land-water boundaries of the area as close as possible, in order to exclude dry cells.
- The grid must be orthogonal, which means that the grid lines should intersect perpendicularly. By making the grid orthogonal, computational expensive transformations terms are left out. A measure for the orthogonality is the cosine of the angle between the grid lines. The cosine has to be smaller than 0.02.
- The grid spacing must be smooth in order to minimize inaccuracy errors in the finite difference operators. A measure for the grid smoothness is the aspect ratio of the grid cells [range 1 to 2] and the ratio of neighbouring grid cell dimensions, which should be less than 1.2 in the area of interest up to 1.4 far away.

An advantage of the staggered grid approach is that boundary conditions can be implemented on the grid in a rather simple way. Boundaries are defined on different locations, closed boundaries are defined through u - or v points, as are velocities, but water levels are defined at water level points (+ points). In Figure F-2 is shown that the velocity points are on the closed boundary whereas the water level points for the boundary are defined outside the grid.

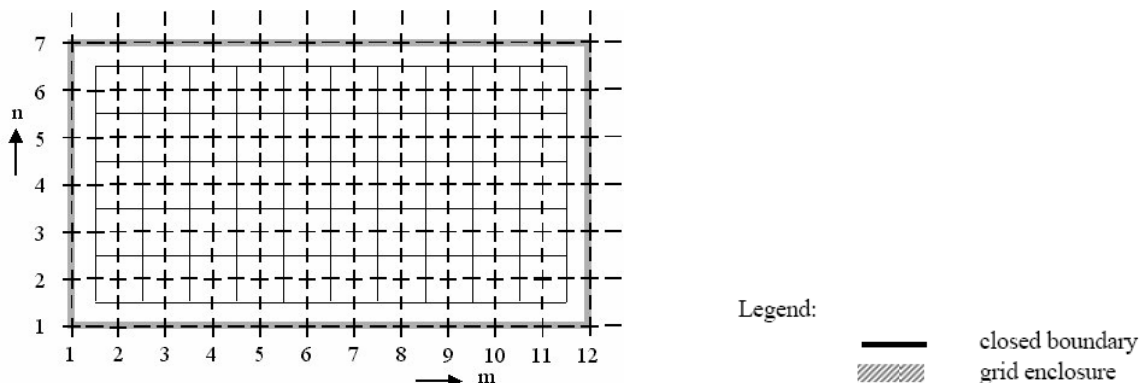


Figure F-2: Grid with grid enclosure and boundary location [DELTA RES, 2010b].

In Delft3D two types of co-ordinate systems in the horizontal can be used:

Cartesian: the co-ordinates are in metres.

Spherical: the co-ordinates are in decimal degrees.

For the Cartesian co-ordinate system a uniform Coriolis force is calculated for the total area. The spherical co-ordinate system calculates the Coriolis force for each cell separately. The spherical co-ordinate is typically used for large areas. For the Langmann reservoir the Cartesian co-ordinate system is used. In the vertical direction two types of grid can be used: the σ -grid and the Z-grid. In the σ -grid the layer thickness varies with the depth, and the number of active layers is constant. In the Z-grid the layer thickness is fixed and the number of active layers varies with the depth, see Figure F-3. In this report no vertical grid is used.

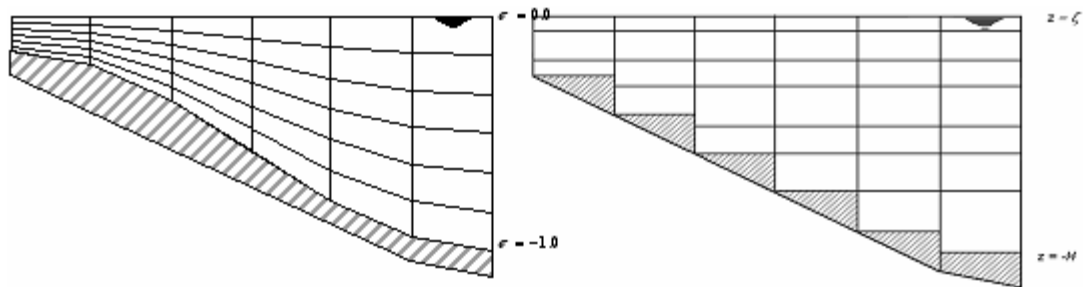


Figure F-3: Vertical grids in Delft3D [DELTA RES, 2010b].

F.3 Assumptions Delft3D

In Delft3D several assumptions and simplifications are made. In this section the assumptions and simplifications for the processes involved are discussed.

General assumptions

As stated in section F.1 the flow is assumed to be incompressible and also hydrostatic pressure is assumed.

Bank erosion

In Delft3D, erosion occurs in a cell, scouring the bed. Bank erosion is not taken into account. This means that a steep scour hole can develop near a dry cell. In order to take the effect of bank erosion into account, a scheme has been implemented that allows redistribution of erosion from a wet cell to the adjacent dry cells. This however does not take the specific mechanisms involved in bank erosion into account.

Drying and flooding

Drying and flooding of grid cells is done by defining a threshold water depth. When the water depth in the model becomes lower than this threshold the cell is set to dry. When the water level becomes higher than the threshold depth the grid cell is set to wet. In the numerical model, the process of drying and flooding is represented by removing grid points from the flow domain that becomes dry and adding grid points when they become wet. Drying and flooding gives a discontinuous movement of the closed boundaries and may generate small oscillations in water levels and velocities. The oscillations introduced by the drying and flooding algorithm are small if

the grid sizes are small and the bottom has smooth gradients. Drying and flooding must be avoided near open boundaries. [DELTARES, (2010a)].

For further assumptions and simplifications there is referred to the Delft3D-FLOW User Manual [DELTARES, (2010a)].

F.4 Sediment transport in Delft3D

Delft3D can model the bed load transport for non-cohesive sediment and the suspended load transport for both non-cohesive and cohesive sediment.

F.4.1 Non-cohesive sediment

In Delft3D, the Van Rijn 1993 formula is used as default for the non-cohesive sediment transport. The Van Rijn 1993 formula includes bed load transport and suspended load transport for waves and currents, where the Van Rijn 1984 formula does not include transport due to waves.

Sediment transport below a certain reference height is treated as bed-load transport and that above the reference height as suspended-load transport. Sediment is entrained in the water column by imposing a reference concentration at the reference height.

$$c_a = 0.015 \rho_s \frac{D_{50} \cdot T_a^{1.5}}{a \cdot D_*^{0.3}} \quad (F.6)$$

where:

c_a = mass concentration at reference height a

T_a = non dimensional bed shear stress

D_* = dimensionless particle diameter

$$D_* = D_{50} \left[\frac{\Delta g}{\nu^2} \right]^{1/3} \quad (F.7)$$

$$T_a = \frac{\mu_c \cdot \tau_{b,cw} + \mu_w \tau_{b,w} - \tau_{cr}}{\tau_{cr}} \quad (F.8)$$

$$\tau_{cr} = (\rho_s - \rho_w) g D_{50} \theta_{cr} \quad (F.9)$$

The transfer of sediment between the bed and the flow is modelled using sink and source terms acting on the near-bottom layer that is entirely above Van Rijn's reference height. This layer is called the kmx-layer, see Figure F-4. In the layers below the kmx-layer the sediment concentrations are assumed to adjust quickly to the same concentration as the kmx-layer. The source and sink terms are given by the erosion flux due to the upward diffusion and the deposition flux due to sediment settling. The source and sink terms are calculated each half time-step. In order to determine the required sink and source terms for the kmx-layer the concentrations and

concentration gradient at the bottom of the kmx-layer need to be approximated. A standard rouse profile is used.

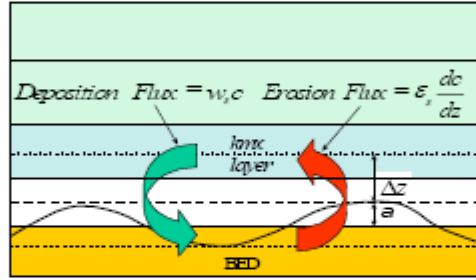


Figure 11.3: Schematic arrangement of flux bottom boundary condition

Figure F-4: Source and sink flux [DELTAES, 2010a].

Total source and sink terms are:

$$\begin{aligned}
 \text{Source} &= \alpha_2 c_a \left(\frac{\varepsilon_s}{\Delta z} \right) \\
 \text{Sink} &= \left[\alpha_2 \left(\frac{\varepsilon_s}{\Delta z} \right) + \alpha_1 w_s \right] c_{kmx}
 \end{aligned} \tag{F.10}$$

where the source and sink terms are both positive. For a complete description reference is made to the Delft3D flow manual [DELTAES (2010a)].

Van Rijn 2004

In Delft3D the Van Rijn 2004 formula can be used. The 2004 formula is an update of the 1993 formula and primarily involves the inclusion of predictors for the bed roughness and refinement of the predictors for the suspended sediment size and the near-bed concentration and the extension of the model to the clay and silt range [WALSTRA *et al*, 2004 and VAN RIJN *et al*, 2007].

The new formula includes a larger range of fine sediments from 8.0 to 2.000 μm , while the lower limit of the Van Rijn 1993 is 64 μm [VAN RIJN, 2007b].

An important difference in the Van Rijn2004 formula is that in the formula the effect of cohesion on the critical bed-shear stress is taken into account, where in VAN RIJN 1993 the critical conditions for initiation of motion according to Shields is used, which is only valid for non-cohesive sediment. The difference between the two is that in the Shields formula the critical bed shear stress decreases with decreasing particle size, while in the new formula the critical shear stress decreases for higher particles sizes, but does not further decrease for smaller particle sizes and even increase in bed-shear stress occurs due to the effect of cohesion, see Figure F-5. In the figure the red dashed line is the line for non-cohesive sediment. The blue lines are including the influence of the cohesion. The dark blue line, with a value of $\gamma=1.5$, is used in the model.

$$\tau_{cr,bed} = (c_{gel} / c_{gel,s}) (D_{sand} / D_{50})^y \tau_{cr,o} < 62 \mu\text{m} \tag{F.11}$$

where:

C_{gel} = Gelling concentration. [g/L]

D_{sand} = 62 μm smallest particle size of non-cohesive bed. [m]

$C_{gel,s}$ = Dry bulk density by volume or mass. [g/L]

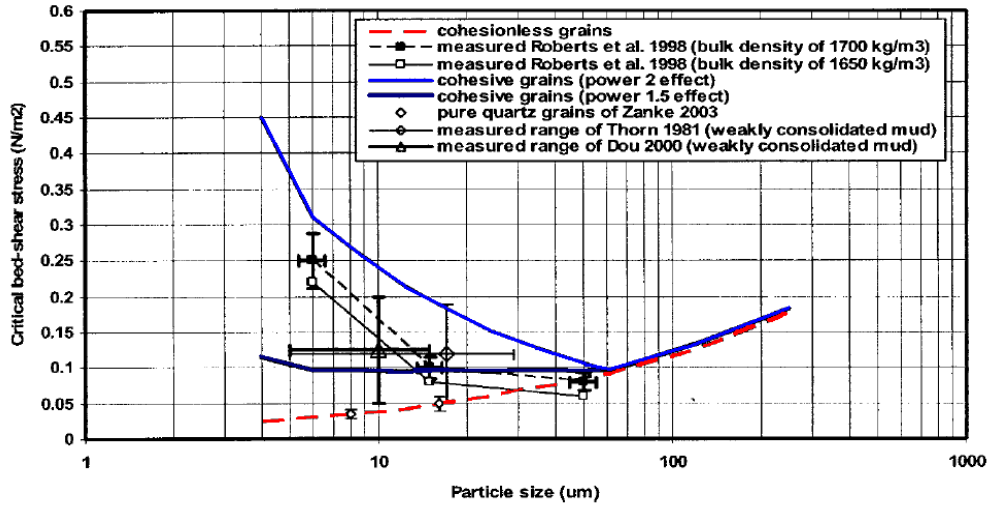


Figure F-5: Effect of cohesive forces on critical bed-shear stress of fine sediment beds [Modified from VAN Rijn 2007a].

Engelund- Hansen

The Engelund-Hansen formula is a formula for total transport. The transport includes bed load as suspended load, but no wash load.

The formula is originally meant for bed load transport but was found to be well applicable for total transport with relative fine sediment where suspended load plays an important role.

The formula of Engelund and Hansen for (transport without pores) can be written as:

$$s = 0.05 \frac{u^5}{\sqrt{g} C^3 \Delta^2 D_{50}} \quad (\text{F.12})$$

The formula can only be used when the following conditions are met:

$$\begin{aligned} \frac{w_s}{u_*} < 1 & \quad \text{with} \quad u_* = \sqrt{g} / C \cdot u \\ 0.19 \text{ mm} < D_{50} < 0.93 \text{ mm} & \\ 0.07 < \theta < 6 & \quad \text{with} \quad \theta = u_*^2 / \Delta g D \end{aligned} \quad (\text{F.13})$$

where:

S = Sediment transport per unit width, excluding pores [m²/s]

u	=	Flow velocity	[m/s]
u_*	=	Shear velocity	[m/s]
θ	=	Shields parameter	[-]
D_{50}	=	Median grain size of bed material	[m]
w_s	=	Fall velocity	[m/s]

F.4.2 Cohesive sediment

For cohesive sediment the Partheniades-Krone formula is used in Delft3D [DELTAIRES, 2010a]. The Partheniades-Krone formula consists of two formulas; one for erosion and one for deposition.

$$E = M \cdot \left(\frac{\tau}{\tau_{cr,e}} - 1 \right) \quad \text{for } \tau > \tau_{cr,e} \quad (\text{F.14})$$

$$E = 0 \quad \text{for } \tau \leq \tau_{cr,e}$$

$$D = \omega_s \cdot C_b \cdot \left(1 - \frac{\tau}{\tau_{cr,d}} \right) \quad \text{for } \tau < \tau_{cr,d} \quad (\text{F.15})$$

$$D = 0 \quad \text{for } \tau \geq \tau_{cr,d}$$

where:

E	=	Erosion flux	[kg/(m ² .s)]
D	=	Deposition flux	[kg/(m ² .s)]
M	=	Erosion parameter	[kg/(m ² .s)]
w	=	Fall velocity	[m/s]
C_b	=	Average sediment concentration	[kg/m ³]
$\tau_{cr,e}$	=	Critical shear stress, erosion	[N/m ²]
$\tau_{cr,d}$	=	Critical shear stress, deposition	[N/m ²]
τ	=	Bed shear stress	[N/m ²]

In Delft3D, the critical shear stresses, the erosion parameter, the initial sediment layer thickness, the wet density, the dry density and the settling velocity must be specified, see Table F.1.

Parameter		Lower limit	Upper limit	Default
Dry density mud	[kg/m ³]	100	3000	500
Settling velocity	[mm/s]	>0.0	30	0.25
Critical shear stress deposition	[N/m ²]	0	1000	1000
critical shear stress erosion	[N/m ²]	0.001	100	0.5
Erosion parameter	[kg/(m ² .s)]	0.0	1	0.0001
Initial bed layer thickness mud	[m]	0.0	10	0.05
Reference density hindered	[kg/m ³]	100	Max.	1600
Specific density	[kg/m ³]	100	4000	2650

Table F.1: Sediment parameters in Delft3D

In VAN RIJN 2005 the range of the erosion parameter M is said to be between 0.00001 and 0.005 kg/m².s. The critical shear stress for erosion ranges from 0.05 to 0.15 N/m². The critical shear stress